Statistica Sinica **19** (2009), 1439-1462

DETECTABILITY OF CONVEX-SHAPED OBJECTS IN DIGITAL IMAGES, ITS FUNDAMENTAL LIMIT AND MULTISCALE ANALYSIS

Xiaoming Huo and Xuelei (Sherry) Ni

Georgia Institute of Technology and Kennesaw State University

Abstract: Given a convex-shape inhomogeneous region embedded in a noisy image, we consider the conditions under which such an embedded region is detectable. The existence of low order-of-complexity detection algorithms is also studied. The main results are (1) an analytical threshold (of a statistic) that specifies what is detectable, and (2) the existence of a multiscale detection algorithm whose order of complexity is roughly the optimal $O(n^2 \log^2(n))$.

Our analysis has two main components. We first show that in a discrete image, the number of convex sets increases faster than any finite degree polynomial of the image size n. Hence the idea of *generalized likelihood ratio test* cannot be directly adopted to derive the asymptotic detectability bound. Secondly, we show that the maximally embedded hv-parallelogram is at least 2/9 of the convex region (in area). We then apply the results of hv-parallelograms in Arias-Castro, Donoho, and Huo (2005) on detecting convex sets. Numerical examples are provided.

Our results have potential applications in several fields, which are described with corresponding references.

Key words and phrases: Convex sets, detectability, image detection, white-noises.

1. Introduction

Detectability is a fundamental problem in many image processing tasks. It is to determine whether detecting an object via computer is *doable*. Furthermore, when it is doable, what is an appropriate order of complexity for the associated algorithm? Regarding detecting the presence of a geometric object in an image with additive Gaussian noises, Arias, Donoho and Huo (2005) proved a range of powerful results: for a given class of geometric objects, the asymptotic threshold of the detectability is a multiplier of $2\sqrt{\log(n)}$, where the image size is n by n. For many classes, the efficient detection algorithm can have orders of complexity such as $O(n)$ or $O(n^2)$.

It is useful to consider an illustration at this point. Figure 1.1 (a) contains a convex set in a square and Figure 1.1 (b) presents the same convex set in a noisy Gaussian random field in the same square. The detectability problem is to ask: when is the convex set detectable and what is the lowest order of complexity for

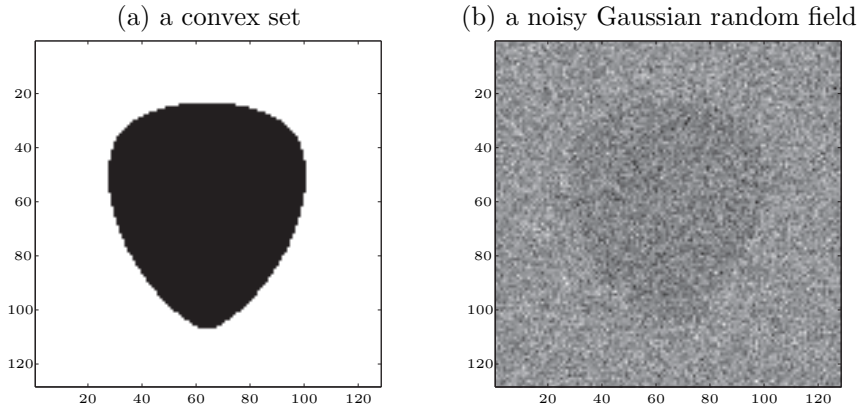

Figure 1.1. A convex set (a) and its embedding in a random field (b).

the detecting algorithms? A statistical formulation of the above is as follows. The intensity at each pixel follows a normal distribution. Inside the convex set, the normal mean is a positive constant (which makes the pixel darker in the above figure); while outside, the normal mean is zero.

Detectability plays a key role in many applications. In the processing of cryo-EM images, due to the low doses of electron that can be applied to the specimen, the signal-to-noise ratio can be extremely low. Before any image processing tasks are applied, one should ask: does the image have the quality to provide any useful information. Detectability addresses this issue. Moreover, a cryo-EM image can be contaminated. Detectability can be utilized to detect the presence of such contaminations. In processing satellite images, due to the resolution of these images, certain tasks, e.g., detecting the presence of a certain class of targets, may not be doable. Detectability can be adopted to decide if a satellite image matches a quality requirement. More applications will be discussed later.

A detection problem is equivalently a hypothesis testing problem. We have a simple null hypothesis and a composite alternative hypothesis. We would like to characterize a neighborhood of the null hypothesis, such that when a subcase of the alternative hypothesis is inside (resp., outside) this neighborhood, it can not (resp., can) be reliably distinguished from the null hypothesis. The key in finding such a neighborhood of the null hypothesis is to study the statistical distribution of the test statistic when the null hypothesis is assumed to be true. The content of this paper can be summarized as follows:

- The infeasibility of adopting the generalized likelihood ratio test is revealed by the study of the cardinality of the convex sets in an n by n image. We give a recursive formula to compute the number of convex sets. From this

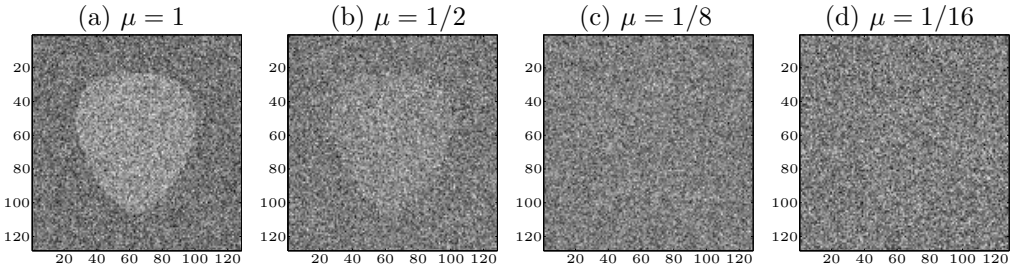

Figure 1.2. A convex object in a white-noise image with $\mu = 1, 1/2, 1/8$, and $1/16$, respectively.

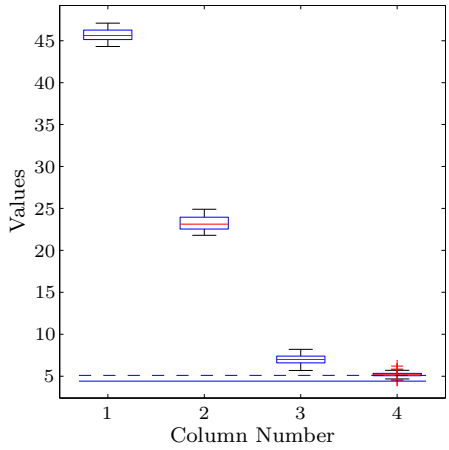

Figure 1.3. Boxplots of the test statistics in four cases that are illustrated in Figure 1.2.

formula, it can be argued that the number of convex sets grows faster than any finite-degree polynomial of n.

- The efficiency of the multiscale detection approach via hv-parallelograms is analyzed by studying the minimax proportion of an hv-parallelogram included in a convex set. We show that the proportion is a constant $2/9$. Hence we provide a method that has the same asymptotic testing power as detecting convex sets directly. However, it has much lower order of complexity.

To see how our result can be utilized in determining detectability, consider the four figures in Figure 1.2. In each figure, a convex region is embedded in a white-noise image. Inside the convex region, the pixel intensities are i.i.d. random variables that satisfy $N(\mu, 1)$. Outside, the pixel intensities satisfy $N(0, 1)$. Note that when $\mu = 0$, we claim no embedded object. The values of μ are in the titles of subfigures. When we have $\mu = 1$ or $1/2$, the convex object is

clearly visible. When $\mu = 1/8$ or $1/16$, the convex object can barely be found. According to our result, to determine the existence of an embedded convex object, an enumeration of all possible convex subsets is not feasible. However, it is doable to compute the maximal test statistic for all hv-parallelograms. The definition of hv-parallelogram will be given later. The computation is of low order of complexity—$O(n^2 \log^2(n))$, where the image size is n by n. The maximal test statistic is then compared with a threshold, which can be obtained either analytically, or empirically. If the maximal statistic is significantly larger than the threshold, we claim that there is an embedded convex object. For each value of μ, we generate 30 random images like those in Figure 1.2. An X^*-statistic (which will be defined later) is computed for each noisy image. The boxplots of the X^*-statistics are shown in Figure 1.3; Each column corresponds to one case (i.e., one value of μ) that is illustrated in a subfigure of Figure 1.2. The solid horizontal line is the theoretical threshold $2\sqrt{\log(n)}$ that is given in Arias, Donoho and Huo (2005). The dashed line is the 90th percentile of the X^*-statistics when $\mu = 0$ with $1,000$ repetitions. It is not surprising that in the first two cases—when $\mu = 1, 1/2$—the boxplots are way above the threshold lines, indicating strong evidence of an embedded convex object. A more interesting case is when $\mu = 1/8$. The boxplot is still apparently above the threshold lines. However visually, it is hard (or even impossible) to observe any embedded object in the noisy image (referring to Figure 1.2 (c)). When $\mu = 1/16$, the embedded object is not detectable: the test statistic is not significantly above the theoretical thresholds. In other words, nobody will be able to detect those objects unless additional information regarding the object is known.

This paper is organized as follows. Section 2 discusses a detection approach that is based on the generalized-likelihood-ratio-test principle, counts the number of convex sets in a digital image, and shows the impracticability of this approach. Section 3 describes the multiscale approach to detect rectangles or hv-parallelograms, computes the minimax proportion of an hv-parallelogram in a convex set, and consequently demonstrates its effectiveness. Simulations are described in Section 4. Section 5 discusses potential applications and relation to other works. A brief conclusion and some discussions are furnished in Section 6.

2. Formulation and a Direct Approach via Likelihood Ratios

We describe our formulation in Section 2.1. A likelihood ratio based detection approach is described in Section 2.2. Section 2.3 proves an infeasibility result.

2.1. Statistical model

To describe the problem, we first establish some notations for a digital image. An $n \times n$ digital image has double indices: (i, j), $0 \le i,\ j \le n - 1$. Each pair of

indices indicates a pixel of the image. A subset of pixels is denoted by Ω, i.e., $\Omega \subset \{(i,j), 0 \le i,j \le n-1\}$. A pixel p is called a *boundary pixel* of Ω, iff (if and only if) it belongs to Ω and one of its neighbor (up, down, left, or right) is outside of Ω. Ω is a convex set if and only if for any two points $x, y \in \Omega$, the line segment connecting x and y is inside the Ω. More rigorous definition for convex sets in a digital image will be given later, when we consider more specific detection approaches.

For a pixel p (with indices (i,j)), let $X(p)$ (or $X(i,j)$) denote the intensity of the image at p, i.e., (i,j). We have

$$X(p) \overset{\text{independent}}{\sim} \begin{cases} N(0,\sigma^2), & \text{if } p \notin \Omega, \\ N(\mu,\sigma^2), & \text{if } p \in \Omega, \end{cases}$$

where $N(\mu,\sigma^2)$ stands for a normal distribution with mean μ and standard deviation σ. An illustration of such sampled image is in Figure 1.1 (b). For future convenience, in this paper we assume $\sigma = 1$. That is, if the image has no embedded signal (i.e., the image is a white noise image), then $X(i,j) \sim N(0,1)$, for all $0 \le i,\ j \le n-1$. This situation is defined as the *null hypothesis* (denoted by H_0). On the other hand, if there is a subset of pixels (denoted by Ω) satisfying that for a constant $\mu > 0$, $X(i,j) \sim N(\mu,1)$ when pixel $(i,j) \in \Omega$, and $X(i,j) \sim N(0,1)$ when pixel (i,j) is outside Ω, then Ω is an "embedded" object. Such a case is defined as the *alternative hypothesis* (denoted as $H_a(\Omega,\mu)$). Note that by varying subset Ω and the value of parameter μ, there are infinite number of possibilities for the alternative hypotheses. The objective of our detection problem is to decide whether or not such an object Ω exists. More specifically, how large should the value of μ and the area of Ω be so that the corresponding alternative hypothesis can be distinguished from the null hypothesis.

2.2. Likelihood ratio based approach

In the statistical model established above, we consider the following hypothesis testing problem:

$$\begin{aligned} H_0 :&\quad X(i,j) \sim N(0,1) \text{ for all } 0 \le i,j \le n-1; \\ H_a(\Omega,\mu) :&\quad X(i,j) \sim N(\mu,1) \text{ for some } \mu > 0 \text{ when } (i,j) \in \Omega. \end{aligned}$$

In this paper, we are interested in the case when Ω is a convex set. The following is an approach that can be easily derived. A useful reference regarding this is Arias, Donoho and Huo (2005). The analysis is based on an asymptotic viewpoint.

First, if Ω and μ are given, we have a simple null hypothesis versus a simple alternative. Define

$$X(\Omega) = \sum_{(i,j)\in\Omega} \frac{X(i,j)}{\sqrt{|\Omega|}},$$

where $|\Omega|$ is the number of pixels in Ω. Under H_0, it is not hard to derive that $X(\Omega) \sim N(0,1)$, while under $H_a(\Omega,\mu)$, we have $X(\Omega) \sim N(\mu\sqrt{|\Omega|},1)$. Hence, one can easily conduct the likelihood ratio test of H_0 against $H_a(\Omega,\mu)$ by asking if $X(\Omega) > \tau$, for a threshold τ.

For the composite alternative hypothesis, where $\mu(>0)$ and Ω are both unknown, it is straightforward to consider the maximum among all $X(\Omega)$'s (denoted by X^*). That is, we consider

$$X^* = \max_{\Omega\in\mathcal{F}_n} X(\Omega), \tag{2.1}$$

where $\mathcal{F}_n$ denotes the collection of all the subsets that are under consideration. For example, when we consider the problem of detecting a convex set, the $\mathcal{F}_n = \{\text{all convex sets in an } n\times n \text{ image}\}$.

Now we derive a detection rule so that for the simple null and the composite alternative, the type-I error probability (i.e., Prob(reject $H_0|H_0$)) converges to 0 as the image size n goes to infinity. Given a constant $\tau > 0$, and taking advantage of a property of $N(0,1)$, we know that under H_0,

(1) for any Ω, $P(X(\Omega) > \tau) < (1/\tau)e^{-(1/2)\tau^2}$ (Pollard (1984, p.191));
(2) $P(X^* > \tau) \le |\mathcal{F}_n| \cdot P(X(\Omega) > \tau) \le |\mathcal{F}_n|(1/\tau)e^{-(1/2)\tau^2}$. The first inequality is due to Bonferroni. The second one is a direct substitution. Here $|\mathcal{F}_n|$ is the cardinality of the set $\mathcal{F}_n$.

Notice that if $\tau^* = \sqrt{2\log|\mathcal{F}_n|} \to +\infty$, then under H_0, $P(X^* > \tau^*) \to 0$. This gives us a powerful hypothesis testing method for the probability of the type-I error of this test goes to zero. On the other hand, considering a subset Ω within which there is a nonzero mean μ, we have $X(\Omega) \sim N(\mu\sqrt{|\Omega|},1)$. If the mean of this normal distribution $\mu\sqrt{|\Omega|} > \tau^*$ (respectively, $\mu\sqrt{|\Omega|} < \tau^*$), such a subset will (respectively, will *not*) be distinguishable from the null. Hence, the aforementioned choice of $\tau^* = \sqrt{2\log|\mathcal{F}_n|}$ gives a threshold on when a subset is *detectable*. Note the above argument implies an asymptotic argument: we omit the notion of $n \to \infty$.

Now we explain why a polynomial expression for the size of set $\mathcal{F}_n$ (i.e., $|\mathcal{F}_n|$) could be useful in determining the asymptotic detectability of convex sets. If the cardinality of set $\mathcal{F}_n$ can be a polynomial of image size n, i.e., for an integer $k > 0$, $|\mathcal{F}_n| = O(n^k)$ (or $\lim_{n\to+\infty}(|\mathcal{F}_n|/n^k) = \text{constant}$), then $\tau^* = C_1\sqrt{2k\log n}$,

where C_1 is a constant. Note that to increase the value of τ^* by a factor of 10, the value of n needs to be increased to n^{100}. The slow growth of τ^* when $|\mathcal{F}_n|$ is a polynomial is an interesting feature of this type of detection problems. In summary, the existence of a polynomial formula for the quantity $|\mathcal{F}_n|$ is of strong interest to us.

2.3. The infeasibility

We show that the aforementioned proposal is infeasible. We first establish a definition for convex sets in digital images. Note that due to the discreteness of the problem, there are other ways to define a convex set.

Definition 1. (convex set) A set Ω is convex iff

1. there exists a close chain of pixels: (a_1, b_1), (a_2, b_2), $\cdots$, (a_k, b_k), and (a_1, b_1), which belong to Ω, and their centers form the vertices of a convex non-degenerated polygon;
2. $\forall p \in \Omega$, the center of p is inside or on the boundary of the above mentioned polygon, and vice versa.

We have clarified the importance of the cardinality of convex sets in an $n \times n$ digital image for evaluating the detectable threshold τ^*. We hope that the cardinality can be expressed in a polynomial of image size n. However, this is not true.

Theorem 2. *Under the above definition of a convex set, the number of convex sets increases faster than any finite degree polynomial of image size n, as $n \to \infty$.*

This result implies that the approach we introduced in the previous section for determining the asymptotic threshold of the detectability of convex sets cannot work. However, we would like to point out that, even though Theorem 2 states that the number of convex sets is not polynomial, it would still be possible to have $\tau^* \sim \sqrt{\log(n)}$. In other words, the nonexistence of a polynomial formula merely invalidates a sufficient condition. The result $\tau^* \sim \sqrt{\log(n)}$ can still be true. In fact, Arias, Donoho and Huo (2005) gives a result of this kind. We refer to that paper for further details. Apparently, such a result *cannot* be derived by counting the number of convex sets.

The proof of Theorem 2 is in Appendix A, see also Ni (2005). The proof is easy to read, not requiring any advanced knowledge in mathematics. The key idea in the proof is establishing an inequality (referring to (A.4)), from which, Theorem 2 becomes provable. After our work, we discovered that the number of convex sets is $\exp\{cn^{2/3}\}$, see Bárány (2002). Such an advanced result confirms our finding.

3. A Multiscale Approach via Hv-parallelograms

Detecting the presence of a convex set in a Gaussian random field is considered further. A multiscale strategy described in Arias, Donoho and Huo (2005) can have the order of complexity $O(n^2 \log^2(n))$ for detecting an hv-parallelogram in an n by n noisy image. So, instead of detecting convex sets directly, we can detect hv-parallelograms that are embedded in convex regions with a positive Gaussian mean. We prove that 2/9 is the minimax proportion of an hv-parallelogram included in a convex set. Such a constant indicates the effectiveness of a multiscale detection method. Section 3.1 reviews the multiscale approach for detecting hv-parallelograms. Section 3.2 gives the main result of the hv-parallelogram-based method.

3.1. Multiscale detection

In this section, we detect a more basic shape—hv-parallelogram—as a surrogate for convex sets. It is relatively easy to compute the $X(\cdot)$-statistic for the new geometric objects. By investigating the relationship between an hv-parallelogram and a convex set, we can build a method to find an inhomogeneous convex region indirectly.

The hv-parallelogram was introduced in Arias, Donoho and Huo (2005). We give the definition and some related information.

Definition 3. (hv-parallelogram) An h-(resp. v-) parallelogram is a parallelogram having two sides horizontal (resp. vertical) and its horizontal (resp. vertical) projection to the y- (resp. x-) axis on a Cartesian plane is a dyadic interval.

Without loss of generality, we assume that the size of the image, n, is 2^m for some integers m. We transfer the index set of pixels from $\{0, \ldots, n-1\}$ to $\{0, 1/2^m, 2/2^m, \ldots, 1 - 1/2^m\}$.

Definition 4. (dyadic interval) Interval (a, b) is a dyadic interval if and only if there exist two non-negative integers s and ℓ, $s \le m$ and $\ell < 2^s$, such that $a = \ell/2^s$ and $b = (\ell + 1)/2^s$.

We reformat the testing scheme as follows. Take

$$X(i,j) \sim \begin{cases} N(0,1), & \text{if } x \notin \Omega, \\ N(\mu,1), & \text{if } x \in \Omega, \end{cases}$$

where $\mu > 0$ and Ω is a convex set. Given a region $\widetilde{\Omega}$, we can calculate

$$X(\widetilde{\Omega}) = \sum_{(i,j)\in\widetilde{\Omega}} \frac{X(i,j)}{\sqrt{|\widetilde{\Omega}|}},$$

where $|\widetilde{\Omega}|$ denotes the number of pixels inside the set $\widetilde{\Omega}$. If set $\widetilde{\Omega}$ does not intersect with the "high activity" convex set Ω (i.e., $\widetilde{\Omega} \cap \Omega = \emptyset$), we have $X(\widetilde{\Omega}) \sim N(0,1)$. Otherwise, we have

$$X(\widetilde{\Omega}) \sim N\left(\mu \cdot \frac{|\widetilde{\Omega} \cap \Omega|}{\sqrt{|\widetilde{\Omega}|}}, 1\right).$$

In Section 2, we chose the detection region $\widetilde{\Omega}$ to be a convex set. In this section, we focus on hv-parallelograms. That is, we calculate

$$\widetilde{X}^* = \max_{\widetilde{\Omega} \text{ is an hv-parallelogram}} X(\widetilde{\Omega}). \tag{3.1}$$

It can be shown that $\widetilde{X}^*$ is upper bounded by a quantity which is a function of n. Specifically, if

$$\begin{aligned} H_0 : &\quad X(i,j) \sim N(0,1) \text{ for all } 0 \le i,j \le n-1; \\ H_a(\widetilde{\Omega}, \mu) : &\quad X(i,j) \sim N(\mu,1) \text{ for some } \mu > 0 \text{ when } (i,j) \in \widetilde{\Omega}, \end{aligned}$$

it can be shown as in Arias, Donoho and Huo (2005) that there exists a constant Γ_n,

$$\frac{\Gamma_n}{\sqrt{2\log(n^2)}} \to 1,$$

such that, as $n \to \infty$, we have

$$P\{\widetilde{X}^* > \Gamma_n | H_0\} + P\{\widetilde{X}^* < \Gamma_n | H_a\} \to 0.$$

That is, if we observe a $X(\widetilde{\Omega})$ that is larger than Γ_n, the presence of an embedded hv-parallelogram can be claimed.

At resolution n (i.e., given an n by n image), there are $O(n)$ dyadic intervals, including both vertical and horizontal directions. For each dyadic interval, there are at most $O(n^3)$ hv-parallelograms: $O(n)$ options for each lower corner, and the height of the parallelogram adds another $O(n)$ possibilities. Hence the total number of the hv-parallelograms is $O(n^4)$, much lower than the cardinality of all the convex sets.

Hence, within $O(n^4)$ operations, we can detect the significant hv-parallelograms in an $n \times n$ image. Actually, a lower order algorithm can be derived by using a multiscale methodology with the help of Beamlets and Beamlet algorithms (Donoho and Huo (2002)). We omit the details and only mention the results with the emphasis that detecting hv-parallelogram can be done efficiently.

Note that we are interested in detecting convex sets, not simple parallelograms. We should ask whether the above detecting rule can be adopted for

convex sets. Furthermore, how to adopt? We give the answer in the following section.

3.2. The minimax proportion of embedded Hv-parallelograms

In this section, we analyze the relationship between an hv-parallelogram and a convex set.

Theorem 5. *For any convex set, there exists an included h- or v- parallelogram that occupies at least* $2/9$ *of the convex set. Moreover, the constant* $2/9$ *cannot be increased.*

A formal proof is lengthy and tedious. We refer to an online downloadable technical report—Ni and Huo (2005); see also Ni (2005).

Recall that we consider all the h- and v- parallelograms and have the new statistics $\widetilde{X}^*$ and $X(\widetilde{\Omega})$ as in (3.1). Comparing with X^* and $X(\Omega)$ in (2.1), we can easily verify that if there exists an inhomogeneous convex region Ω_0, which leads to $X(\Omega_0) \sim N(\mu\sqrt{|\Omega_0|}, 1)$, then this Ω_0 includes an hv-parallelogram $\widetilde{\Omega}_0$ that occupies at least $2/9$ of Ω_0 in area, and $X(\widetilde{\Omega}_0) \sim N(\mu\sqrt{|\widetilde{\Omega}_0|}, 1)$. Thus

$$E(X(\widetilde{\Omega}_0)) \geq \sqrt{\frac{2}{9}} E(X(\Omega_0)).$$

Hence an powerful test can be based on the comparison between $(3/\sqrt{2})\widetilde{X}^*$ and Γ_n given earlier.

From the above, we claim that the asymptotic detectability threshold for convex sets is $2\sqrt{\log(n)}$, while the order of complexity for the efficient algorithm is $O(n^2 \log^2(n))$.

4. Simulations

We start with a synthetic study that was mentioned in the Introduction. We then provide an application in cryo-EM image processing (Section 4.2).

4.1. The synthetic example in introduction

At the end of Introduction, we described a simulation study with four levels of μ. There could be an embedded convex object; if a pixel is on the embedded object, its intensity satisfies $N(\mu, 1), \mu \neq 0$; if not, pixel intensity satisfies i.i.d. $N(0, 1)$. For clarity, bigger versions of the noisy images for the four cases given in Figure 1.2. are replotted in Figure 4.9. Our objective is to determine whether or not an embedded convex object exists. Based on previous analysis, if $\widetilde{X}^*$ (which is defined in (3.1)) is well above a threshold, we can declare the existence of a

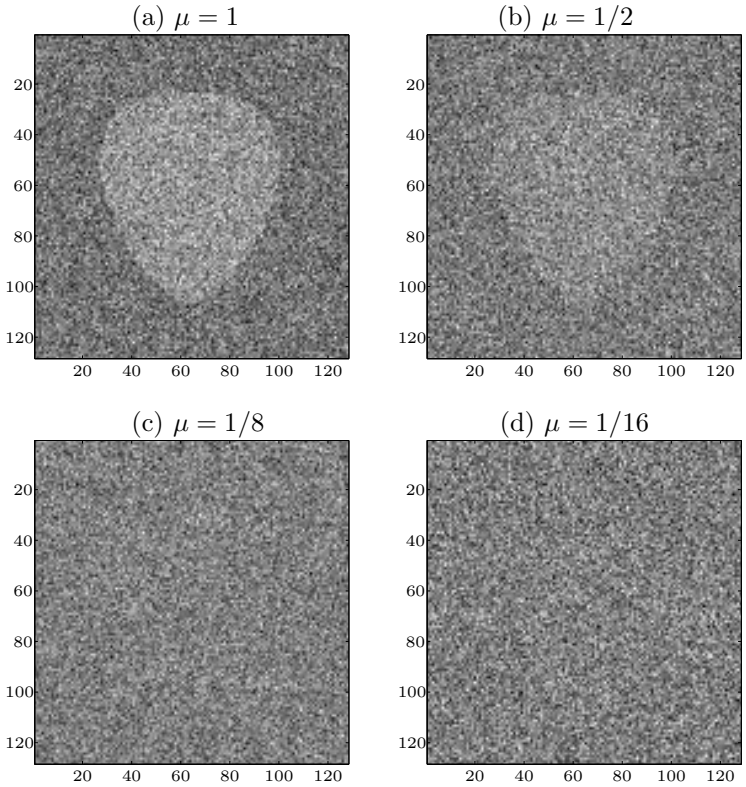

Figure 4.9. A convex object in a white-noise image with $\mu = 1, 1/2, 1/8$, and $1/16$, respectively. Bigger images are shown here.

convex object. Consequently we can design an approach to uncover this object—this part is not included in the present paper. If the $\widetilde{X}^*$ is close to the threshold, then the problem itself is in principle unsolvable.

A value, based on an image size n going to infinity, of the threshold is $2\sqrt{\log(n)}$. However, for finite n, the analytical expression may not apply. One can alternatively use simulations to determine the threshold. In Figure 4.10, we plot the histogram of $\widetilde{X}^*$ based on 1,000 simulations with $\mu = 0$. The theoretical value $(2\sqrt{\log(n)})$ is plotted as a vertical line. The key observation is that if there is no embedded object (i.e., the image is a pure white-noise image), then the value of $\widetilde{X}^*$ is almost never more than 6.0. The two horizontal lines in Figure 1.3 were based on this finding. From Figure 1.3, we can declare that with this shape of convex set, when $\mu \geq 1/8$, the embedded convex object is detectable, and it can be detected via hv-parallelograms. When $\mu = 1/16$ or smaller, the detection problem is not doable—the noisy image is too much like a white-noise image.

Note that when $\mu = 1/8$, it is impossible to see any embedded object in the

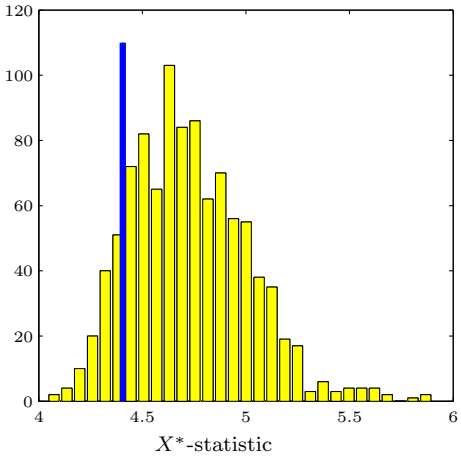

Figure 4.10. A histogram for X^*-statistics when $\mu = 0$, based on 1,000 simulations. The vertical line is the position of $2\sqrt{\log(n)}$—the theoretical threshold.

noisy picture (Figure 4.9 (c), but our analysis demonstrates that the underlying convex region is still detectable.

It is reasonably fast to compute the $\widetilde{X}^*$-statistic. On a laptop running Windows XP with 2.26 GHz CPU and 1.92 GB of RAM, in Matlab, the running time for calculating the $\widetilde{X}^*$-statistic for a 128 by 128 image is about 2 seconds.

4.2. A case from CryoEM image processing

The dtectability problem is motivated by challenges in cryo-electron microscope (cryoEM) image processing. CryoEM has become an indispensable tool in biology to study molecular structures. Figure 4.11 (a) presents a typical cryoEM imagery of a molecule. Because these imageries are taken by electron microscopes, improving image resolution (or signal-to-noise-ratio) would require an increment of voltage of an electron beam. Such an action could burn the biological sample. On the other hand, since the images are taken at nano-scale, it is extremely costly to improve the image quality. Statistical computing is apparently a cost-effective alternative. One big problem in CryoEM is to select imageries that are *useful*. In statistics, *usefulness* can be defined as saying that the imagery contains sufficient information so that it can be utilized. Under the framework that is presented in this paper, a useful imagery must be significantly different from the background noise (Figure 4.11 (b)) in CryoEM.

A background cryoEM image can be approximated by a white-noise; though the existence of the *contrast transfer function* in cryoEM images makes this assumption not completely true. Our numerical study on this is still preliminary.

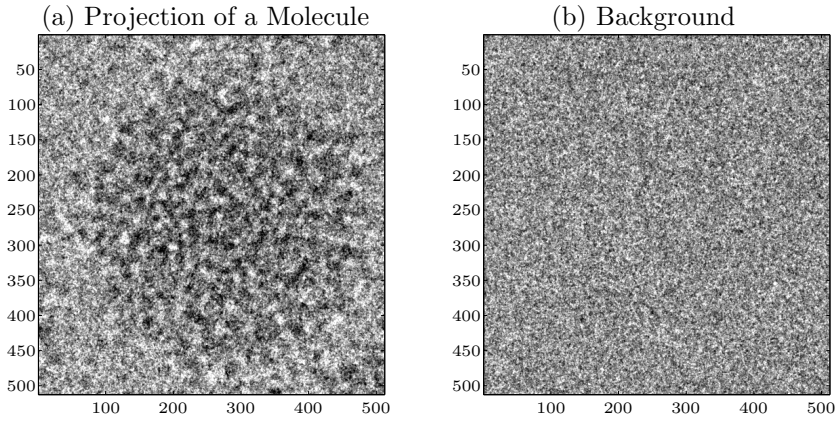

Figure 4.11. Noisy cryo-EM images. (a) A typical cryo-electron microscope imagery—projection of a molecule; (b) pure background noise.

Assuming that the background is nearly white-noise, we can compute the aforementioned $\widetilde{X}^\star$-statistics. After standardizing the two noisy pictures in Figure 4.11, we found that the corresponding $\widetilde{X}^\star$-statistics were 73.4 (for the molecular projection) and 14.5 (for the background), respectively. Notice that the latter is much larger than the theoretical threshold ($2\sqrt{\log 512} = 4.9953$) that is derived from white-noise images. Such an inconsistency is likely due to the effect of the contrast transfer function. Discussion regarding removing such an effect is going to be lengthy and beyond the scope of this paper. The fact that the former $\widetilde{X}^\star$-statistic is nearly 5 times large as the latter indicates the promise of such an approach.

5. Related Works and Applications

We discuss related works (Section 5.1) and potential applications (Section 5.2).

5.1. Related works

Useful constants in other scenarios. The constant 2/9 is a major technical achievement of this paper. Similar works, regarding the constants related to multiscale methods in other problems, can be found in, e.g., Huo (2005a,b). In Huo (2005a), the lower bound of the proportion of a maximally embedded beamlet is shown to be 1/7. In Huo (2005b), the minimax correlation between a line segment and a beamlet is proved to be $2^{-3/4}$. The beamlet has been described in Arias, Donoho and Huo (2005). The above constants are useful in deriving threshold regarding line segment detectability.

Fundamental detectability in Bayesian estimation. Our approach can be classified as a frequentist approach. We consider a simple null hypothesis versus a composite alternative hypothesis. The objective is to characterize a neighborhood of the null hypothesis, such that when the alternative is inside (resp., outside) this neighborhood, the alternative is indistinguishable (resp., distinguishable) from the null hypothesis. Another approach is to weight the alternatives by a prescribed prior distribution, i.e., a Bayesian framework. Researchers have successfully applied it to detection problems, see Yuille and Coughlan (2000) and Yuille, Coughlan, Wu and Zhu (2001). They derived the fundamental bound of detectability below which the target is not detectable, and vice versa. Such a bound depends on a constant that is a function of the distributions determined by the detection problem. Due to the differences in formulation, there will be different applications of both types of theorems. It is interesting to compare them and to discuss where a particular type of result should be used.

5.2. Applications

Constantly improved imaging technology and cheaper and better computers give rise to demands and wishes to use digital images as tools for evaluation and analysis. Automatic analysis and extraction of information from an image becomes more and more important in many fields. In most of these applications, data (images) are collected by standard sensors such as cameras and radars. The collected images are analyzed for the detection and the recognition of the targets, either stationary or moving, with unknown background. Detecting an inhomogeneous region with a convex shape in a noisy environment is one of many problems. We discuss several potential applications in the following.

In electron cryomicroscopy Van Heel, Gowen, Matadeen, Orlova, Finn, Pape, Cohen, Stark, Schmidt, Schatz and Patwardhan (2000) and Yu (2003)), accurate and automatic particle detection from cyro-electron microscopy (Cryo-EM) images is very important for fast and correct reconstruction of macromolecular structures. Since achieving high-resolution reconstruction often requires over hundreds of thousands of particles, it is extremely important to design a fast and automatic algorithm for particle detection. Detectability could lead to a quality measure of cryoEM images.

Filament detection and image alignment in Cryo-EM. Automated filament identification plays an important role in the image reconstruction of helical objects from electron micrographs (Zhu, Carragher, Kriegman, Milligan. and Potter (2001)). Due to the necessity of using low doses of electrons to image the specimen, the signal-to-noise-ratio is low in these images. A three-level perceptual organization algorithm is proposed in Zhu et al. (2001). What is of interest is

how strong the signal-to-noise-ratio should be so that the filament identification can be considered doable. Answering this question will lead to the detectability problem that is studied in our paper. We notice the difference in the problem formulation. However, many analytical techniques developed here can be utilized in both problems.

Contamination detection. The presence of contaminants can severely harm the performance of a particle detection algorithm. Detecting contaminants is necessary, due to the low signal-to-noise-ratio of cryoEM images. In the literature of contaminant detection, e.g., Zhu, Carragher and Potter (2004), convex shaped regions have been considered. Even though Zhu et al. (2004) consider an algorithmic approach, instead of the detectability problem that is studied here, their use of convex hulls lends us support for considering convex objects.

In geomorphology (Kim, Muller and Morley (2004), Celebi, Aslandogan and Bergstresser (2005), and Xu, Jackowski, Goshtasby, Yu, Roseman, Bines, Dhawan and Huntley (1999)), impact crater detection and crater size frequency counting have a very high priority in Extra Terrestrial Mapping and planetary chronological research. For example, in the Mars exploration, the existence of numerous impact craters in one area will provide witness to the evolving surface process on Mars and may help us find the geological evidence for running water on (or just below) the surface of Mars. Hence, automation of crater detection is an important initial step toward making more efficient the work of the analyst facing huge volumes of images produced by missions.

In medical science (Kalender, Polacin and Suess (1994)), for accurate diagnosis, it is crucial to accurately locate and isolate the lesions in a brain or a skin image. Detection of lesions in the early stages considerably reduces morbidity and mortality. However, automated detection is a challenging task for several reasons: (a) low contrast between the lesion and its surroundings, (b) reflections and shadows due to wrong illumination, and (c) artifacts such as skin texture, air bubbles, and hair. The detectability problem is: how different the signal of the lesion should be, so that the detection is a solvable problem.

Qi (2004) and Qi and Huesman (2001) adopt a different formulation than ours. We consider hypothesis testing, in which the null hypothesis is *simple* and the alternative hypothesis is *composite*, while Qi (2004) and Qi and Huesman (2001) consider a *simple* null hypothesis versus a *simple* alternative hypothesis. They quantify the detectability as the area under the ROC curve (UAC), where the ROC stands for 'receiver operating characteristic.' They further establish the relation between the UAC and the signal-to-noise-ratio (SNR): the UAC changes monotonically with the value of SNR. Consequently, they derive a closed form approximate for SNR for the purpose of characterizing detectability. The closed

form is obtainable under specific situations, e.g., when the estimate is a maximum *a posteriori* (MAP).

The formulation of the lesion detection problem provides us with a potential future research topic. Under a similar framework, we can study our detectability problem; their definition of detectability demonstrates that our formulation is not the only aspect of the detection problem.

Ellipses detection. Ellipses detection (Bennett, Burridge and Saito (1999)) is a special case of convex region detection. In medical images, ellipses detection has been used in automated detection of bronchial abnormalities on computed tomography (CT) lungs (Chabat, Hu, Hansell and Yang (2001)). Ellipses are convex. Hence the content of this paper can be utilized to decide when ellipses detection algorithm can work.

Rooftop and building detection. Rooftop detection is an important step of building detection and description in aerial images (Noronha and Nevatia (1997)). Maloof, Langley, Binford, Nevatia and Sage (2003) give a survey on incorporating learning algorithms in this problem. In a handcrafted system, like the one in Noronha and Nevatia (1997), detecting parallelograms is an important intermediate step. This coincides with our usage of hv-parallelograms, although the purposes are not completely identical. All methods rely on some preprocessing steps, such as edge detection and grouping in finding buildings' boundaries. Note that boundaries are highly fragmented; when multiple images are utilized, as in Noronha and Nevatia (1997), the results of boundary detector can be unreliable. In our framework, we can analyze the condition under which the rooftop detection is feasible. Such a condition will depend on the quality of the images, as well as how the rooftops differ from the clutters. Many specific domain knowledge should be taken into account, as in Noronha and Nevatia (1997) and Maloof et al. (2003). Here, we merely mention the possibility as a future research topic. We point out that the area under the ROC curves is also used in Maloof et al. (2003) to evaluate different classifiers.

In summary the concept of detectability has many potential applications.

6. Conclusion and Discussion

Detectability is an important concept in contemporary image processing. We show that the threshold of detectability is *not* derivable via the traditional generalized likelihood ratio test, because the number of convex subsets is not a polynomial of the image size. However, a multiscale approach initiated in Arias, Donoho and Huo (2005) can give the asymptotic threshold. A key in adopting the threshold in Arias, Donoho and Huo (2005) to convex sets is the minimax ratio 2/9, which is derived in this paper. Such a constant determines

the effectiveness of numerical implementation of a multiscale method that utilizes hv-parallelograms in detection of convex objects. Potential applications are discussed. Literature pointers are provided.

We discuss some key assumptions in our analysis framework, as well as their impacts on the practicality of the proposed approach. We have assumed that the pixel intensities are random variables, which are *independent* and *normally distributed*. It appears that both assumptions can be relaxed to some degree. A key fact that we utilized in deriving the asymptotic threshold is the inequality on the tail probabilities of a weighted partial sum—see item (1) shortly after (2.1). It is known that a similar inequality can be established for independent sub-Gaussian random variables. We may not require the pixel intensities to be identically distributed—in a white-noise image, the pixel intensities are identically distributed. Such a change of formulation can dramatically change the presentation of the current paper. The purpose of this paper is to introduce the multiscale approach—and the use of hv-parallelograms.

The assumption that the underlying object is *convex* shaped may be too restrictive in some applications. This paper is concerned with convex objects, while the methodology may be modified for other geometric objects (including non-convex ones). The convex assumption is general and, under it, we can derive some insightful theoretical results. On the other hand, we do not expect our results to be applicable in all practical problems.

We make a homogeneous assumption—the pixel intensities inside (or outside) the embedded region have identical distributions. Such an assumption makes some asymptotic thresholds (e.g., $2\sqrt{\log(n)}$ for convex regions) possible. As mentioned above, we may relax the assumption of identical distribution; however, in the current framework, some conditions on the homogeneity seem unavoidable. This may oversimplify practical problems. At this stage, we consider our work more of a theoretical analysis than an applied project.

An interesting fact associated with multiscale approaches—in this case, the adoption of hv-parallelograms—is that multiscale methods render the correct asymptotic rate; on the other hand, a direct application of the Bonferroni's approach cannot. A reason behind such a fact is that the hypotheses (particularly the alternative hypotheses) are dependent since the embedded regions may overlap with each other. A direct application of the Bonferroni's approach ignores such a dependency. At the same time, it is unclear how to incorporate the dependence structure into a straightforward Bonferroni's framework. The multiscale decomposition—such as the decomposition of convex sets into hv-parallelograms, see Arias, Donoho and Huo (2005) for more technical details—turns out to be the effective way to count the complexity in the hypothesis testing problem. Specifically, the multiscale decomposition gives the correct rate of degrees of freedom

in the corresponding hypotheses testing problem, hence leads to the accurate asymptotic rate. The computational advantage of a multiscale approach has been widely recognized as well.

Acknowledgement

This project is partially supported by NSF Grants 0604736 and 0700152.

Appendix A: Proof of Theorem 2

We need some new notation. (Recall that a convex set is determined by a convex polygon whose vertices are the centers of some boundary pixels.) Let $a_1 = \min\{i : (i,j) \in \Omega\}$, $b_1 = \min\{j : (i,j) \in \Omega\}$, $b_2 = \max\{j : (i,j) \in \Omega\}$, and $a_2 = \max\{i : (i,j) \in \Omega\}$. The rectangle $[a_1, a_2] \times [b_1, b_2]$ is the minimum bounding rectangle of the convex set Ω. Let $t_1 = a_2 - \min\{i : (i,b_1) \in \Omega\}$, $t_2 = b_2 - \min\{j : (a_2,j) \in \Omega\}$, $t_3 = \max\{i : (i,b_2) \in \Omega\} - a_1$, and $t_4 = \max\{j : (a_1,j) \in \Omega\} - b_1$. An illustration is given in Figure 6.12.

We need another notation: $H(a,b)$. For $a, b \geq 0$, a sequence of points—$(0,0)$, (c_1,d_1), (c_2,d_2), …, (c_ℓ,d_ℓ), (a,b)—determines a convex curve iff the chain of line segments that connect the centers of these pixels, in the same order, is convex. If this convex curve lies within the boundary of the right triangle with vertices $(0,0), (a,0)$, and (a,b) (boundary is included), we call it a *restricted convex curve* between $(0,0)$ and (a,b). Apparently, for a restricted convex curve, we must have $0 \leq c_1 \leq c_2 \leq \cdots \leq c_\ell \leq a$ and $0 \leq d_1 \leq d_2 \leq \cdots \leq d_\ell \leq b$. More restrictively, if $\forall \ell, c_\ell < a$, we claim that this restricted convex curve does not with the vertical line $i = a$. The total number of restricted convex curves that do not intersect with the vertical line $i = a$ is denoted by $H(a,b)$. Without much effort, one can derive (i) $H(0,b) = 0$, for $b \geq 0$; (ii) $H(a,0) = 1$, for $a \geq 1$; and (iii) $H(1,b) = 1$, for $b \geq 1$. We would like to draw attention to the fact that, because $c_\ell < a$, the last segment ((c_ℓ,d_ℓ) to (a,b)) *cannot* be the vertical line passing through point (a,b). Furthermore, notice that under our definition, $H(a,b)$ and $H(b,a)$ could be unequal, for example, $H(0,b) \neq H(b,0)$ when $b \geq 1$.

Recall Figure 6.12. It is not hard to prove that the following is the total number of convex sets under our definition:

$$\sum_{k_1,k_2=1}^{n} (n-k_1)(n-k_2)G(k_1,k_2), \tag{A.1}$$

where $k_1 = a_2 - a_1$, $k_2 = b_2 - b_1$, and $G(k_1,k_2)$ is the number of convex sets whose minimal bounding rectangle is of size $k_1 \times k_2$. One can verify that, assuming $H(0,0) = 1$, we have

$$G(k_1,k_2) = \sum_{\substack{0\leq t_1,t_3\leq k_1,\\ 0\leq t_2,t_4\leq k_2}} H(t_1,k_2-t_2)H(t_2,k_1-t_3)H(t_3,k_2-t_4)H(t_4,k_1-t_1). \tag{A.2}$$

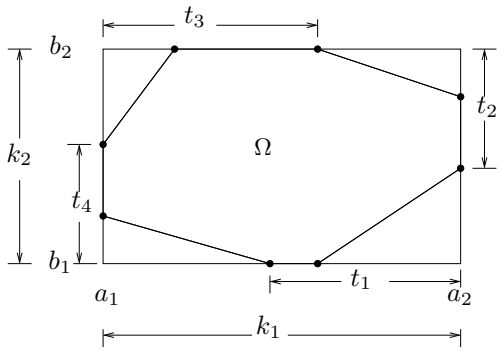

Figure 6.12. Notations for the second case.

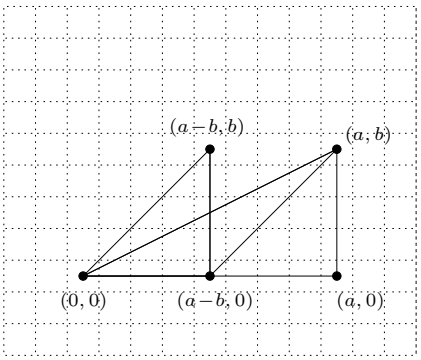

Figure 6.13. Illustration for the proof of Lemma 6.

Now the importance of $H(a,b)$ in our analysis is clear. To get our main result, we proceed by proving the following lemmas regarding $H(a,b)$.

Lemma 6. *The number of restricted convex curves between points* $(0,0)$ *and* (a,b)*,* $a > b$*, and with slopes* < 1*, is* $H(a-b,b)$*. Here, "slopes" refer to the slopes of line segments that make up the convex curve.*

This can be proved similarly to Lemma 6. We omit the details and only give the illustration in Figure 6.14.

Proof. Readers can refer to Figure 6.13 for an illustration of the proof. First of all, the convex curves satisfying the condition of the Lemma will lie within the triangle $((0,0),(a-b,0),(a,b))$, without touching the edge between $(a-b,0)$ and (a,b), except at the last point. For simplicity, we use C_1 to denote this set of convex curves . At the same time, $H(a-b,b)$ is the number of restricted convex curves between $(0,0)$ and $(a-b,b)$ that do not intersect with line $i = a-b$. We use C_2 to denote this set of convex curves. We want to show $|C_1| = |C_2|$. Note

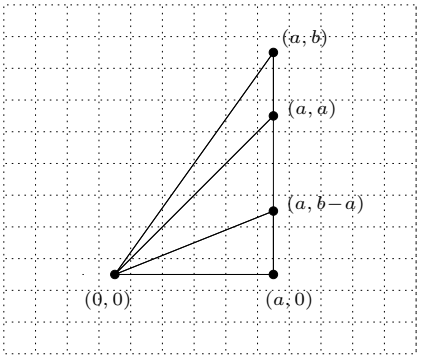

Figure 6.14. Illustration for the proof of Lemma 7.

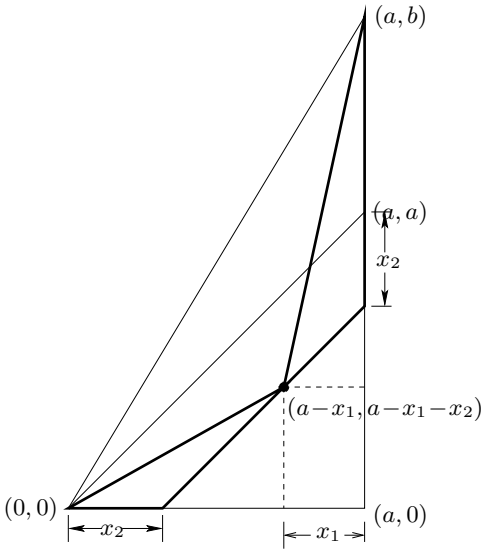

Figure 6.15. Illustration of the proof of Lemma 8.

that $\forall\ \{(0,0),(c_1,d_1),\ldots,(c_l,d_l),(a,b)\} \in C_1$, one can easily verify $\{(0,0),(c_1 - d_1,d_1),\ldots,(c_l-d_l,d_l),(a-b,b)\} \in C_2$. On the other hand, $\forall\ \{(0,0),(e_1,f_1),\ldots,(e_m,f_m),(a-b,b)\} \in C_2$, $\{(0,0),(e_1+f_1,f_1),\ldots,(e_m+f_m,f_m),(a,b)\} \in C_1$. Hence, there exists a one-to-one mapping between the curves in C_1 and the curves in C_2. The Lemma is proved.

Lemma 7. *The number of restricted convex curves that are between points* (0.0) *and* (a,b), $a < b$, *with slopes* ≥ 1, *and not intersecting with line* $i = a$, *is* $H(a,b-a)$.

Lemma 8. Recursive Rule) *For $b \geq a > 0$,*

$$H(a,b) = H(a,b-a) + \sum_{\substack{x_1+x_2\leq a,\\ x_1,x_2\geq 1}} H(x_2, a-x_1-x_2)H(x_1, b-a+x_2), \quad \text{(A.3)}$$

Proof. We describe it graphically. Refer to Figure 6.15.

For any curve that can be counted into $H(a,b)$, there are two possibilities (and only these two):

1. **Case 1.** The slopes of the curve are all ≥ 1.
2. **Case 2.** One of the vertices of the curves, (p^1, p^2), which is the center of a pixel p, satisfies the following: starting from the left, until reaching its center, the slope of the convex curve is strictly less than 1; after this vertex, the slope of the convex curve is at least 1.

Hence,

$$\begin{aligned} H(a,b) &= \#\{\text{curves from Case 1}\} + \#\{\text{curves from Case 2}\} \\ &= \#\{\text{curves from Case 1}\} \\ &\quad + \sum_p \#\{\text{curves ending at } p\} \cdot \#\{\text{curves starting from } p\}. \end{aligned}$$

Under the first circumstance, the restricted convex curves have been analyzed in Lemma 7. So $\#\{\text{curves from Case 1}\} = H(a, b-a)$.

Under the second circumstance, since the slopes of the convex curve before (p^1, p^2) (including the edge ending at p) are strictly less than 1, (p^1, p^2) should be strictly under the line that connects $(0,0)$ and (a,a), i.e., $p^2 < p^1$. We can rewrite $p^2 = p^1 - x_2$, where $x_2 \geq 1$, illustrated in Figure 6.15. Also, since the convex curve cannot intersect with the vertical line $i = a$, p^1 should be strictly less than a. So we can rewrite $p^1 = a - x_1$, with integer $x_1 \geq 1$, also illustrated in Figure 6.15. The center of pixel p becomes $(a - x_1, a - x_1 - x_2)$, $x_1 \geq 1$, $x_2 \geq 1$. At last, because $p^2 \geq 0$, we have $x_1 + x_2 \leq a$. Actually, one can check from Figure 6.15 that (p^1, p^2) must lie strictly within the triangle with vertices $(0,0)$, (a,b), and $(a,0)$, or lie on the line segment connecting $(0,0)$ and $(a,0)$ (excluding the ending points). The geometric meanings of x_1 and x_2 are illustrated in Figure 6.15. Conditions $x_1 \geq 1$, $x_2 \geq 1$, and $x_1 + x_2 \leq a$ give an enumeration of all the possible positions of p.

Now, we have

$$\begin{aligned} H(a,b) = H(a,b-a) + \sum_{\substack{x_1+x_2\leq a, x_1, x_2\geq 1\\ p=(a-x_1, a-x_1-x_2)}} &\#\{\text{curves ending at } p\} \\ &\times \#\{\text{curves starting from } p\}. \end{aligned}$$

From Lemma 6, the number of restricted convex curves between $(0,0)$ and $(a-x_1, a-x_1-x_2)$, with slopes <1, is $H((a-x_1)-(a-x_1-x_2), a-x_1-x_2) = H(x_2, a-x_1-x_2)$.

Consider the last term, $\#\{\text{curves ending at } p\}$. By switching the origin $(0,0)$ to $(a-x_1, a-x_1-x_2)$, we observe that the number of restricted convex curves between $(a-x_1, a-x_1-x_2)$ and (a,b), with slopes ≥ 1, is equal to the number of convex curves between $(0,0)$ and $(a-(a-x_1), b-(a-x_1-x_2)) = (x_1, b-a+x_1+x_2)$, with slopes ≥ 1. The latter, from Lemma 7, is $H(x_1, b-a+x_2)$.

From the above, the Lemma is proved.

As a direct application of Lemma 8, one can verify the following.

- $H(2,b) = 2 + \lfloor((b-1)/2)\rfloor$, for $b \geq 1$ where $\lfloor x\rfloor$ is the largest integer that is no larger than x. This can be verified from $H(2,b) = H(2,b-2)+1$ for $b \geq 2$, which is stated by Lemma 8, and $H(2,0) = 1$, $H(2,1) = 2$.
- $H(3,b) = H(3, b-3\lfloor(b/3)\rfloor) + 2\lfloor(b/3)\rfloor + \sum_{i=1}^{\lfloor(b/3)\rfloor}(\lfloor((b+4-i)/2)\rfloor - i)$.
- $H(3,1) = 3$, $H(3,2) = 4$, and $H(3,3) = 5$.

Another way to utilize Lemma 8 is to derive the following.

Corollary 9. *For $a \geq 1$, $H(a,a) \geq 1 + (a(a-1))/2$.*

Proof.

$$H(a,a) = H(a,0) + \sum_{\substack{x_1+x_2\leq a\\ x_1,x_2\geq 1}} H(x_2,\cdot)H(x_1,\cdot) \geq 1 + \sum_{x_1=1}^{a-1}\sum_{x_2=1}^{a-x_1} 1 = 1 + \frac{1}{2}a(a-1).$$

Recall that we have $H(1,1) = 1$, $H(2,2) = 2$, $H(3,3) = 5$.

Proof of Theorem 2. From Lemma 8, one can prove for $a > 0$,

$$H(a,b) \geq \frac{b^{a-1}}{a^{2a}}. \tag{A.4}$$

By choosing a large enough and $b = 2a^2$, the right hand side of (A.4) increases faster than any polynomial with a prescribed degree. Verifying (A.4) via (A.3) is a simple exercise. We describe it briefly below.

Proof of (A.4).

- When $b < a$, $H(a,b) > 1 > [(b^{a-1})/(a^{2a})]$.

- When $b \geq a > 0$, from Lemma 8 and induction,

$$\begin{aligned} H(a,b) &= H(a,b-a) + \sum_{\substack{x_1+x_2\leq a,\\ x_1,x_2\geq 1}} H(x_2, a-x_1-x_2)H(x_1, b-a+x_2) \\ &\geq \frac{(b-a)^{a-1}}{a^{2a}} + \sum_{\substack{x_1+x_2\leq a,\\ x_1,x_2\geq 1}} \frac{(a-x_1-x_2)^{x_2-1}}{x_2^{2x_2}} \frac{(b-a+x_2)^{x_1-1}}{x_1^{2x_1}} \\ &\geq \frac{(b-a)^{a-1}}{a^{2a}} + \left[\frac{(b-a)^{a-2}}{(a-1)^{2(a-1)}} + \frac{(b-1)^{a-3}}{(a-2)^{2(a-2)}} + \cdots\right] \\ &> \frac{1}{a^{2a}}\left[(b-a)^{a-1} + \binom{a}{1} a(b-a)^{a-2} + \binom{a}{2} a^2(b-a)^{a-3} + \cdots\right] \\ &= \frac{b^{a-1}}{a^{2a}}. \end{aligned}$$

From (A.1) and (A.2), it is not hard to see that the number of convex sets also grows faster than any finite-degree polynomial of n. Theorem 2 is proved.

References

Arias, E., Donoho, D. L. and Huo, X. (2005). Near-optimal detection of geometric objects by fast multiscale methods. *IEEE Trans. Inform. Theory* **51**, 2402-2425.

Bárány, I. (2002). Random points, convex bodies, lattices. *Proceedings of the International Congress of Mathematicians* **III**, 527-535. Higher Ed. Press, Beijing.

Bennett, N., Burridge, R. and Saito, N. (1999). A method to detect and characterize ellipses using the Hough transform. *IEEE Trans. Pattern Anal. Mach. Intell.* **21**, 652-657.

Celebi, M. E., Aslandogan, Y. A. and Bergstresser, P. M. (2005). Unsupervised border detection of skin lesion images. In *Proceedings of the IEEE International Conference on Information Technology: Coding and Computing*, Las Vegas, NV.

Chabat, F., Hu, X. P., Hansell, D. M. and Yang, G. Z. (2001). ERS transform for the automated detection of bronchial abnormalities on CT of the lungs. *IEEE Transactions On Medical Imaging* **20**, 942-952.

Donoho, D. and Huo, X. (2002). Beamlets and multiscale image analysis. In *Multiscale and Multiresolution Methods* **20** (Edited by s. T. J. Barth, T. Chan and R. Haimes), 149-196. Springer Lecture Notes in Computational Science and Engineering.

Huo, X. (2005a). Exact lower bound for proportion of maximally embedded beamlet. *Appl. Math. Lett.* **18**, 529-534.

Huo, X. (2005b). Minimax correlation between a line segment and a beamlet. *Statist. Probab. Lett.* **72**, 71-81.

Kalender, W., Polacin, A. and Suess, C. (1994). A comparison of conventional and spiral CT: an experimental study on the detection of spherical lesions. *J. Comput. Assist. Tomogr.* **18**, 910-915.

Kim, J. R., Muller, J. P. and Morley, J. (2004). Quantitative assessment of automated crater detection on Mars. In *Proceedings of the XXth ISPRS Congress*, Commission IV, 816-821.

Maloof, M. A., Langley, P., Binford, T. O., Nevatia, R. and Sage, S. (2003). Improved rooftop detection in aerial images with machine learning. *Machine Learning* **53**, 157-191.

Ni, X. S. (2005). New results in detection, estimation, and model selection, Ph.D. thesis, Georgia Institute ofTechnology, Atlanta, GA, available at `http://etd.gatech.edu/`.

Ni, X. S. and Huo, X. (2005). The maximally embedded hv-parallelogram is at least 2/9 of the convex region. Tech. Rep. 23, Georgia Institute of Technology, available at `http://www.isye.gatech.edu/statistics/papers/`.

Noronha, S. and Nevatia, R. (1997). Detection and description of buildings from multiple aerial images. In *Proceedings of the 1997 Conference on Computer Vision and Pattern Recognition* (CVPR '97), 588-594.

Pollard, D. (1984). *Convergence of Stochastic Processes*, Springer-Verlag, New York.

Qi, J. (2004). Analysis of lesion detectability in Bayesian emission reconstruction with nonstationary object variability. *IEEE Transactions on Medical Imaging* **23**, 321-329.

Qi, J. and Huesman, R. H. (2001). Theoretical study of lesion detectability of MAP reconstruction using computer observers. *IEEE Trans. Med. Imaging* **20**, 815-822.

Van Heel, M., Gowen, B., Matadeen, R., Orlova, E. V., Finn, R., Pape, T., Cohen, D., Stark, H., Schmidt, R., Schatz, M. and Patwardhan, A. (2000). Single-particle electron cryo-microscopy: towards atomic resolution. *Quarterly Reviews of Biophysics* **33**, 307-369.

Xu, L., Jackowski, M., Goshtasby, A., Yu, C., Roseman, D., Bines, S., Dhawan, A. and Huntley, A. (1999). Segmentation of skin cancer images. *Image and Vision Computing* **17**, 65-74.

Yu, Z. (2003). 'Particle Picking' website, Tech. rep., The University of Texas at Austin, `http://www.ices.utexas.edu/$\sim$zeyun/pick.htm`.

Yuille, A. L. and Coughlan, J. M. (2000). Fundamental limits of Bayesian inference: order parameters and phase transitions for road tracking. *IEEE Trans. Pattern Anal. Mach. Intell.* **22**, 160-173.

Yuille, A. L., Coughlan, J. M., Wu, Y. and Zhu, S. C. (2001). Order parameters for detecting target curves in images: when does high level knowledge help? *International Journal of Computer Vision* **41**, 9-33.

Zhu, Y., Carragher, B., Kriegman, D. J., Milligan, R. A. and Potter, C. S. (2001). Automated identification of filaments in cryoelectron microscopy images. *J. Struct. Biol.* **135**, 302-312.

Zhu, Y., Carragher, B. and Potter, C. S. (2004). Contaminant detection: improving template matching based particle selection for cryo-electron microscopy. In *Proceedings of the IEEE International Symposium on Biomedical Imaging*, Arlington VA, 1071-1074.

School of Industrial and Systems Engineering, Georgia Institute of Technology, Atlanta, GA 30332, U.S.A.

E-mail:xiaoming@isye.gatech.edu

Department of Mathematics and Statistics, Kennesaw State University, Kennesaw, GA 30144, U.S.A.

E-mail: xni2@kennesaw.edu

(Received December 2007; accepted February 2009)